

Preparation and Optical Properties of Indium Tin Oxide/Epoxy Nanocomposites with Polyglycidyl Methacrylate Grafted Nanoparticles

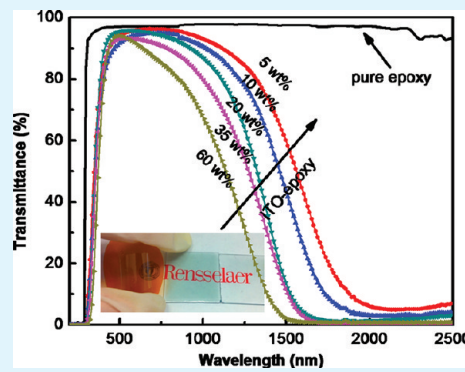
Peng Tao,[†] Anand Viswanath,[‡] Linda S. Schadler,^{*,†} Brian C. Benicewicz,[‡] and Richard W. Siegel[†]

[†]Department of Materials Science and Engineering and Rensselaer Nanotechnology Center, Rensselaer Polytechnic Institute, Troy, New York 12180, United States

[‡]Department of Chemistry and Biochemistry and USC Nanocenter, University of South Carolina, Columbia, South Carolina 29208, United States

ABSTRACT: Visibly highly transparent indium tin oxide (ITO)/epoxy nanocomposites were prepared by dispersing polyglycidyl methacrylate (PGMA) grafted ITO nanoparticles into a commercial epoxy resin. The oleic acid stabilized, highly crystalline, and near monodisperse ITO nanoparticles were synthesized via a nonaqueous synthetic route with multigram batch quantities. An azido–phosphate ligand was synthesized and used to exchange with oleic acid on the ITO surface. The azide terminal group allows for the grafting of epoxy resin compatible PGMA polymer chains via Cu(I) catalyzed alkyne–azide “click” chemistry. Transmission electron microscopy (TEM) observation shows that PGMA grafted ITO particles were homogeneously dispersed within the epoxy matrix. Optical properties of ITO/epoxy nanocomposites with different ITO concentrations were studied with an ultraviolet–visible–near-infrared (UV–vis–NIR) spectrometer. All the ITO/epoxy nanocomposites show more than 90% optical transparency in the visible light range and absorption of UV light from 300 to 400 nm. In the near-infrared region, ITO/epoxy nanocomposites demonstrate low transmittance and the infrared (IR) transmission cutoff wavelength of the composites shifts toward the lower wavelength with increased ITO concentration. The ITO/epoxy nanocomposites were applied onto both glass and plastic substrates as visibly transparent and UV/IR opaque optical coatings.

KEYWORDS: ITO, epoxy, nanocomposite, “click” chemistry, UV/IR shielding



1. INTRODUCTION

With increasing environmental and energy saving concern, optical materials with high visible wavelength transparency as well as high UV/infrared (IR) blocking properties are needed for application as UV/IR shielding windows in automobiles and buildings, contact lenses, and heat mirrors.^{1–5} Nanocomposites using organic polymers and inorganic nanoparticles have attracted significant attention because of their potential for use in optical applications requiring high visible transparency.^{6,7} The properties of the composite materials can be engineered through judicious selection of nanoparticles and polymer. Inorganic nanoparticle/polymer composites with enhanced mechanical, electrical, dielectric, thermal, and optical performance have been reported.⁸ Among the wide variety of available polymers, epoxy resins represent a class of thermosetting polymeric materials with extensive industrial application ranging from coatings to adhesives and the matrixes for composite materials used for electronic and optical devices packaging.⁹ Because they possess superior transmission in the visible range and excellent adhesion with various substrates, epoxy resins are an important optical coating material. Epoxy does not block UV light, but it can be modified to block UV or IR light via addition of appropriate inorganic nanoparticles.^{10,11} Metal oxides with wide band gap are ideal

candidates for UV protection of the organic polymers. Therefore, UV-shielding nanocomposites have been prepared by adding strong UV absorbers (ZnO, TiO₂, and CeO₂ nanoparticles) at low content.⁷ UV-resistant TiO₂/PMMA and ZnO/polystyrene have been prepared with the addition of a small amount of organic ligand.^{12,13} However, most of the previous work has been focused on UV-shielding nanocomposites with thermoplastic polymer matrixes. Only limited work has been performed on both UV and IR blocking energy efficient materials.¹⁴

Tin-doped indium oxide (ITO) was reported to be the most favorable energy efficient material due to its remarkable combination of high transparency in the visible range, high infrared reflectivity, UV-light absorption, and high thermal stability.¹⁵ In most cases, ceramic ITO thin films were fabricated with various techniques including physical vapor deposition, chemical vapor deposition, electron beam evaporation, and magnetron sputtering.^{16–19} These techniques usually have strict requirements on the geometry and structure of the substrates. Often with these techniques, high temperature processing and vacuum equipment are necessary. By comparison, wet chemical

Received: June 29, 2011

Accepted: August 8, 2011

Published: August 08, 2011

deposition of dispersions containing ITO nanoparticles would be preferred for the mass production of coating films due to their low cost, flexibility, and good processability.^{20–25} Indeed, rapid progresses in nonaqueous synthesis of high quality metal oxide nanoparticles enabled the fabrication of ITO nanoparticle polymer composites.^{26–29} However, simply blending nanoparticles with organic polymers usually results in agglomeration of the nanoparticles within the polymer matrixes and loss of optical transparency due to intense light scattering by the agglomerated nanoparticles. Capozzi et al. found that PMMA/ITO nanocomposites prepared by mechanical mixing and compression molding totally lost their optical transparency with 3 wt % loading of ITO nanoparticles.³⁰ The optical transmittance of Al-doped-ZnO/epoxy nanocomposites has also been reported to degrade rapidly even with less than 0.2 wt % loading.¹⁴ Therefore, effective techniques are desired to achieve good dispersion of nanoparticles within organic polymer matrixes and thereby high optical transparency of the composite materials.

It is crucial to have the uniform nanofiller dispersion within the polymer matrix, in particular for the preparation of transparent nanocomposites. Extensive efforts have been made to improve the compatibility between metal oxide nanoparticles and organic polymers. Concentrating sufficient charge on the surface of particles to form an electric double layer was one of the methods to keep particles in dispersion. This scheme typically is limited to systems with highly polar solvents. Steric stabilization is the more favorable dispersion technique. Surface modification with organic capping agents such as silane coupling agents and small molecular ligands has been used to stabilize the dispersion in solvents with moderate success.^{12,13,31–35} However, when the solvent is removed, phase separation between the nanoparticles modified with small ligands and organic polymers occurs. Covalently grafting polymer chains to the surface of inorganic nanoparticles has been considered as one of the most promising techniques to overcome the attraction force between nanoparticles and achieve stabilized dispersion at high concentration.^{36–40} Known for its high efficiency, selectivity, and mild reaction condition, Cu(I)-catalyzed alkyne–azide “click” chemistry has been used to immobilize polymer chains onto inorganic nanomaterials, leading to improved mechanical and dielectric properties of polymer nanocomposites.^{41–45} However, to the best of our knowledge, preparation of transparent optical materials using “click” chemistry has not been reported for combined UV/IR opaque and visibly transparent nanocomposites. In this work, we report the preparation of ITO/epoxy nanocomposites with high visible light transparency and UV/IR blocking using ITO nanoparticles grafted with matrix compatible polymer chains. The polymer chains were attached via a combination of phosphate ligand engineering and alkyne–azide “click” chemistry. The prepared ITO/epoxy nanocomposites can be easily applied on glass and plastic substrates as functional optical coating materials.

2. EXPERIMENTAL SECTION

Materials. Indium(III) acetate (99.99%), tin(II) acetate, oleic acid (90%), oleylamine (70%), and octadecene (90%) were purchased from Sigma Aldrich for ITO nanoparticle synthesis. Tetrahydrofuran (THF) was dried over CaH_2 overnight and distilled before use. Prop-2-ynyl 4-cyano-4-(phenyl carbonothioylthio) pentanoate was synthesized according to previous work.⁴⁶ Azobisisobutyronitrile (AIBN) was purchased from Sigma Aldrich and recrystallized from ethanol before use. Glycidyl methacrylate was passed through a neutral alumina column to remove

the inhibitor before use. POCl_3 (99.99%) and NaN_3 were obtained from Sigma Aldrich. $N,N,N',N''\text{-Pentamethyldiethylenetriamine}$ (PMDETA) and 11-bromo-1-undecanol were purchased from Acros. $\text{Cu}(\text{I})\text{Br}$ (99.999%, Aldrich) was purified with glacial acetic acid and washed with diethyl ether and ethanol before use. Epoxy resin 301-1 was purchased from Epoxy Technology.

Synthesis of ITO Nanoparticles. ITO nanoparticles were prepared through a thermal decomposition of indium acetate and tin acetate under an argon atmosphere using oleic acid and oleylamine as capping agents by modifying the procedures in previous work.^{28,47} Typically, to a 500 mL three-neck round-bottom flask containing 150 mL octadecene, 9 mmol of $\text{In}(\text{Ac})_3$, 1 mmol of $\text{Sn}(\text{Ac})_4$, 15 mL of oleic acid, and 15 mL of oleylamine were added. The mixture was degassed, stirred with a magnetic stir bar, and heated to 120 °C for 1 h with an argon purge. Then, the flask was heated to 300 °C at a heating rate of 10 °C/min, and the solution was refluxed for another 3 h under an argon stream. ITO nanoparticles were obtained by cooling the flask to room temperature, precipitating with acetone, and centrifuging. The obtained particles were easily dispersed into nonpolar solvent such as hexane and chloroform.

Synthesis of Azido-Phosphate Ligand. 11-Azidoundecyl dihydrogen phosphate was synthesized using a simple two-step reaction. First, to a 250 mL round-bottom flask containing 60 mL of DMF, 10 g of 11 bromo-1-undecanol and 3 g of NaN_3 were added. The mixture was stirred with a magnetic stir bar at room temperature for 24 h. The reaction was quenched by adding 50 mL of DI water. 11-Azidoundecan-1-ol (8.5 g) was obtained after extraction with CHCl_3 (30 mL), extraction with DI water (30 mL), drying over sodium sulfate, rotoevaporation, and drying under a vacuum oven overnight. Second, 4.2 g (20 mmol) of 11-azidoundecan-1-ol and 3.11 mL (22 mmol) of triethylamine were added into 60 mL of anhydrous THF in a 250 mL round-bottom flask in an ice bath. Then, 2.07 mL (22 mmol) of POCl_3 was added into the solution dropwise. The solution was stirred for 5 h and quenched with the addition of DI water. The final product, 11-azidoundecyl dihydrogen phosphate (3.8 g), was obtained after completing the extraction and drying process. Fourier transform infrared spectroscopy (FTIR), NMR, and mass spectrometry (MS) were used to determine and analyze the synthesized phosphate ligand.

Click Polymer Chains onto ITO Nanoparticles. A mixture of as-synthesized ITO particles and 11-azidoundecyl dihydrogen phosphate with a weight ratio of 1:1 dispersed in chloroform was subjected to a refluxed stirring at 75 °C overnight. The phosphate treated particles were washed 3 times with ethanol and finally dispersed into THF. Alkyne-terminated poly(glycidyl methacrylate) (PGMA, 20 000 g/mol, PDI = 1.2) was synthesized with a reversible addition–fragmentation chain transfer (RAFT) polymerization technique based on our previous work.^{46,48} In a typical “click” reaction, 0.5 g of phosphate treated ITO particles, 0.4 g of azide-PGMA, and 20 μL of PMDETA ligand were added into 60 mL of anhydrous THF. Ten milligrams of CuBr was added into the flask, and the solution was bubbled with argon gas for 5 min. The flask was transferred into an oil bath at 55 °C for 48 h.

Preparation of ITO Nanocomposites. The PGMA grafted ITO nanoparticles were dispersed in chloroform via sonication. The pure PGMA grafted ITO composites were prepared by casting the dispersion onto a plastic Petri dish and removing the solvent in the oven at 80 °C overnight. ITO/epoxy nanocomposites were prepared by mixing PGMA grafted ITO nanoparticle dispersion with commercial diglycidyl ether of bisphenol A (DGEBA) epoxy resin (Epoxy Technology, 301-1), and curing agent (trimethyl-1,6-hexanediamine). The resultant mixture was coated onto glass and plastic substrates followed by thermal curing at 80 °C overnight.

Characterization. Powder X-ray diffraction (XRD) patterns for ITO nanoparticles were recorded on a Bruker D8 diffractometer using $\text{Cu K}\alpha$ radiation ($\lambda=1.5405 \text{ \AA}$) and operating at an accelerating voltage of 40 kV, in the 2θ range from 10 to 80° (step of 0.01°). FTIR spectra

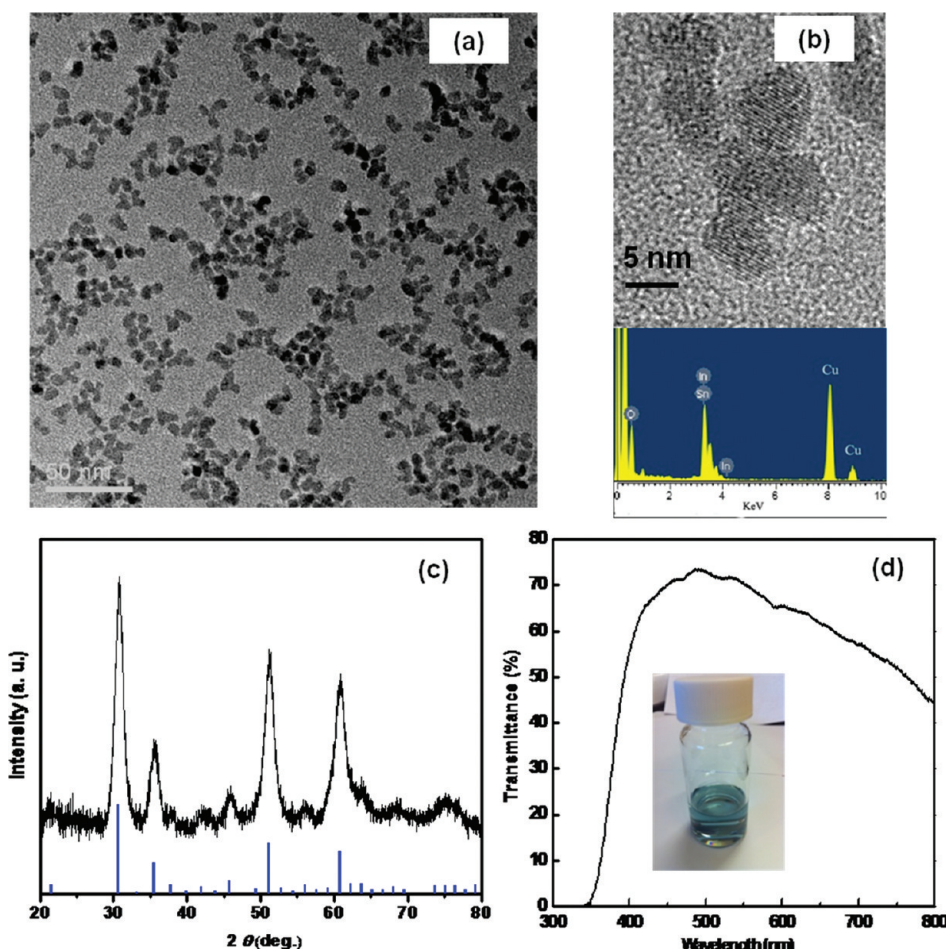


Figure 1. (a) TEM image of synthesized ITO nanoparticles, (b) HRTEM image with TEM-EDS analysis, (c) XRD diffraction pattern, (d) transmittance spectrum of ITO dispersion in hexane (10 mg/mL) measured through a quartz cuvette and inset photograph of green ITO dispersion.

were obtained on a Perkin-Elmer Spectrum One FT-IR Spectrophotometer scanning from 500 to 4000 cm^{-1} with a resolution of 4 cm^{-1} for 10 scans. Thermal gravimetric analysis (TGA) was done on a Perkin-Elmer Series 7 instrument. The sample was heated from 30 to 700 °C under a 60 mL min^{-1} nitrogen flow at a heating rate of 10 °C/min. X-ray photoelectron spectroscopy (XPS) data were acquired with a monochromatic Al K α X-ray source on a PHI 5000 Versa Probe XPS spectrometer. A takeoff angle of 45° from the surface was employed. Transmission electron micrographs (TEM) and X-ray energy dispersive spectroscopy (EDS) spectra were obtained using a JEOL-2010 microscope operating at 200 kV. TEM samples were prepared by cutting ITO-epoxy nanocomposites to 50 nm at room temperature using an RMC PowerTome microtome. The transmittance spectra of nanocomposites were measured with a Perkin-Elmer Lambda 950 ultraviolet-visible-near-infrared (UV-vis-NIR) spectrophotometer.

3. RESULTS AND DISCUSSION

Figure 1a shows the TEM and high resolution transmission electron microscopy (HRTEM) micrographs of the homogeneously distributed as-synthesized ITO nanoparticles. Figure 1b presents a high resolution TEM image of the synthesized ITO nanoparticles. A single crystalline domain within each particle can be clearly observed. The TEM EDS analysis on the ITO particles shows the existence of C, O, In, Sn, and Cu elements. The Cu is due to the copper grid used in the TEM sample holder,

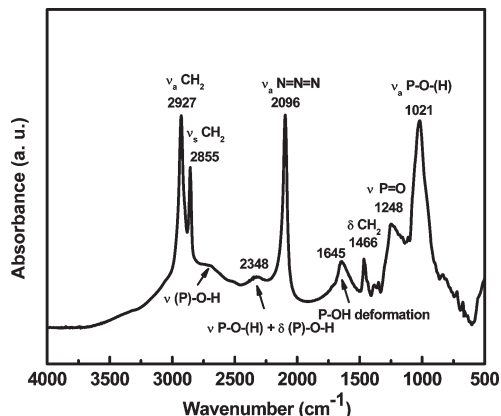
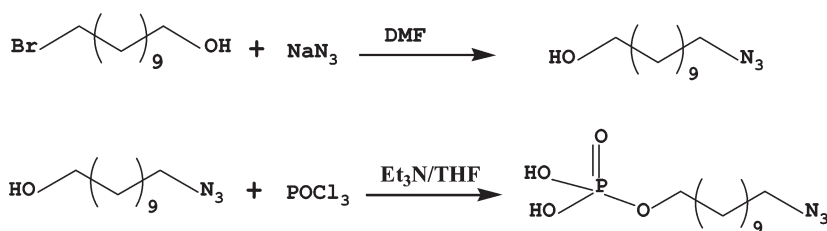
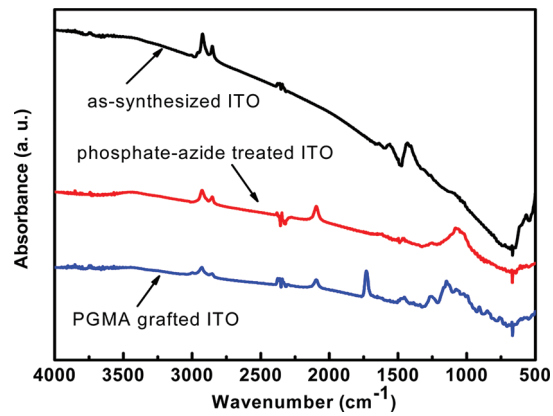
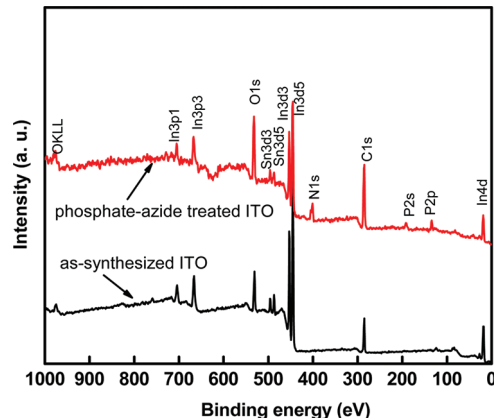
and the C element can be attributed to the presence of the surface capping agent, oleic acid. The atomic ratio of tin and indium is 3.47:31.70, which is in accordance with the prescribed 10 at % doping composition.

Figure 1c displays the XRD pattern of the ITO nanoparticles. All of the detectable diffraction peaks of ITO can be indexed to a pure body-centered-cubic In_2O_3 structure (JCPDS card #: 06-0416). No impurity peaks are found in the sample within the experimental error, indicating successful doping of SnO_2 into the In_2O_3 lattice. Meanwhile, the crystal size of ITO particles was estimated by measuring the broadening of the (222) peak using the Scherrer equation:

$$D = 57.3k\lambda/(\beta \cos \theta) \quad (1)$$

where the shape factor k was taken as 0.9, λ is the wavelength of Cu K α 1 irradiation (1.5405 Å), β is the half-intensity width, and θ is the Bragg angle. The average particle size was estimated to be 6.6 nm, which is consistent with the average particle size of 6.3 nm based on TEM observation.

Figure 1d shows the light green color dispersion of ITO nanoparticles in hexane. As shown in the transmittance result of the ITO dispersion, the ITO nanoparticles have an interband transition near 400 nm and weak absorption in the red region, resulting in a green color. During the reflux process at high temperature, a gradual color change of the solution was observed.

Scheme 1. Synthesis of 11-Azidoundecyl Dihydrogen Phosphate**Figure 2.** FTIR spectrum of 11-azidoundecyl dihydrogen phosphate.**Figure 4.** FTIR spectra of as-synthesized ITO, phosphate-azide treated ITO, and PGMA grafted ITO nanoparticles.**Figure 3.** XPS survey of synthesized ITO and ITO particles treated with phosphate-azide.

When the temperature was raised to 200 °C, initially, clear solution quickly turned from light yellow to orange-yellow. When the temperature reached 300 °C, the transparent yellow mixture gradually turned deep green, indicating successful doping of tin and the formation of ITO with high carrier concentration. Due to surface capping by oleic acid, the synthesized particles were easily dispersed in nonpolar solvent and formed a transparent dispersion. It is worth noting that an important feature of the synthesized particles is their relatively narrow size distribution even with grams of particles per batch yield, evidenced by the TEM images. The high-quality, batch-scalable ITO particle synthetic route would allow for their potential use in industry.

As shown in Scheme 1, the phosphate-azide ligand was synthesized via a two step reaction. Figure 2 shows the full FTIR spectrum of the synthesized 11-azidoundecyl dihydrogen phosphate. The strong absorption around 3000 cm⁻¹ was assigned as asymmetric and symmetric CH₂ vibration from the long alkyl chain. The intense azide band at 2100 cm⁻¹ and characteristic peaks of phosphate in the fingerprint region were also observed. The organophosphates have been reported to be able to bind very strongly to the surface of metal oxides.^{35,49} The original capping agent, oleic acid, on the synthesized ITO particle surface was exchanged with the stronger phosphate binder by refluxing the ITO particles with azido-phosphate ligands overnight. The refluxing process enhances the surface ligand exchange and binding of the stronger phosphates. Figure 3 compares the XPS survey results of both the as-synthesized ITO particles and the phosphate treated particles. After surface treatment with the azido-phosphate ligand, extra N and P peaks due to the azide group and phosphate headgroup, respectively, were detected. Quantitative analysis of the as-synthesized ITO and phosphate treated particles showed a 2.2:23.8 ratio of tin-to-indium, which is also consistent with the TEM EDS results.

The ITO nanoparticles were anchored with a long alkyl chain phosphate ligand, which has an azide terminal group, allowing for the grafting of polymer chains onto the particle surface via a simple and efficient “click” reaction. As shown in Figure 4, the alkyne terminated PGMA chains were successfully grafted onto ITO particles using the “click” chemistry as evidenced by the reduction in azide vibration intensity and the introduction of characteristic peaks from the PGMA polymer such as the carbonyl vibration near 1700 cm⁻¹. After reaction with alkyne-terminated PGMA, the azide peak intensity decreases significantly but not

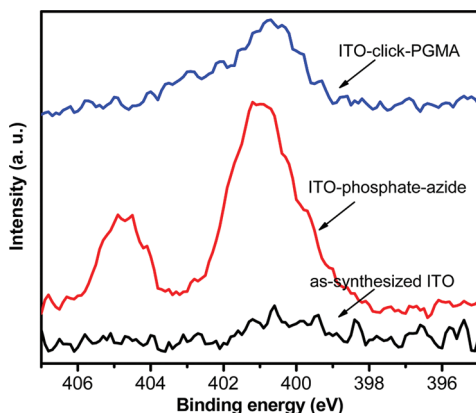


Figure 5. XPS scan of N1S of as-synthesized ITO, phosphate–azide treated ITO, and PGMA grafted ITO nanoparticles.

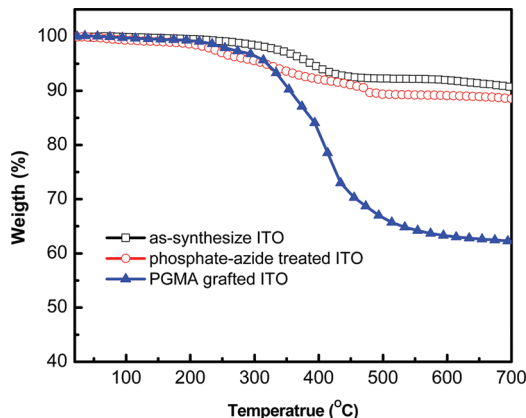


Figure 6. TGA curves of as-synthesized ITO nanoparticles, phosphate–azide treated ITO nanoparticles, and PGMA grafted ITO particles.

completely, which indicates not all the azide groups have reacted. The P–O symmetric vibration can be seen in both the phosphate treated particle sample and the particle with grafted polymer chains. However, the FTIR spectra of ITO samples showed a broad absorbance over almost the complete spectral range, which was due to plasma vibrations and oscillations of conduction electrons in the ITO particles. The strong absorption in the infrared range prevents more detailed analysis with FTIR.

XPS was used to further analyze the click reaction, and the result is shown in Figure 5. The high-resolution peak of the N 1s spectrum shows that no peak was observed for the synthesized ITO particles and there are two peaks at 405 and 401 eV in the phosphate–azide treated ITO sample. Ideally, the azide nitrogen exists in two different oxidation states with a ratio of 1:2, where the high binding energy peak corresponds to the relatively electron poor middle N atom of the azide group.⁵⁰ In our experiment, the ratio of the areas of these two peaks of the phosphate–azide treated ITO sample is approximately 1:3, and the deviation was possibly due to the degradation of the azides during the XPS measurement.⁵¹ After the click reaction, due to the formation of triazole, the peak at 401 eV can still be observed while the peak at 405 eV is not apparent. Fitting the N1s spectrum in the ITO-click-PGMA sample showed that the resultant spectrum could be best fitted with peaks at 405 and 401 eV with an area ratio of 1:5, which means around 50% of the

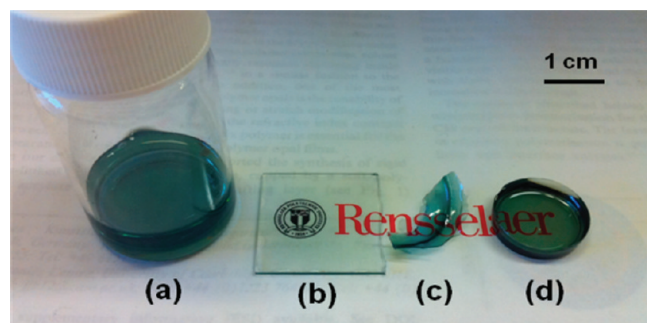


Figure 7. Photographs (a) ITO/PGMA dispersion in chloroform, (b) ITO/PGMA coating on glass slides, (c) 100 μm thick ITO/PGMA composites after removal of solvent (60 wt % ITO loading), (d) ITO/epoxy composites (20 wt % ITO loading, 3 mm thick).

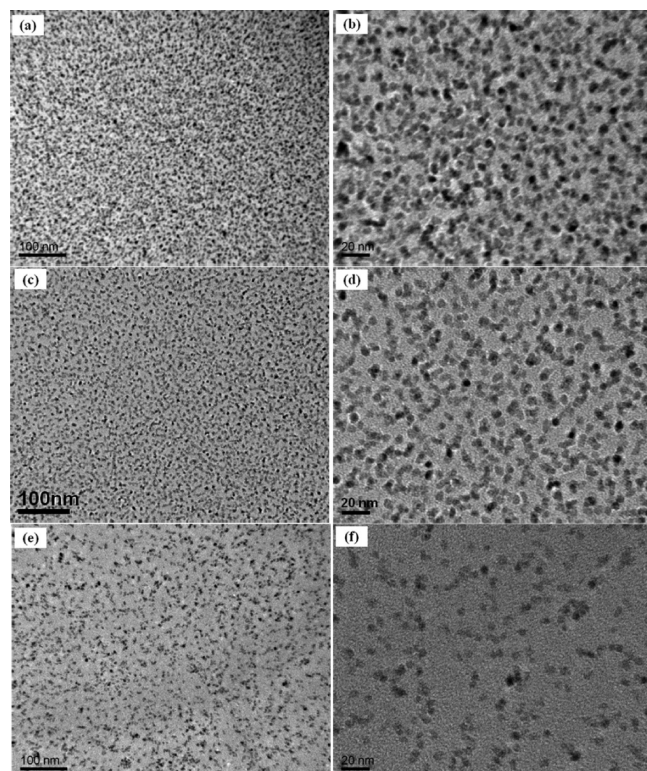


Figure 8. TEM image of ITO/epoxy nanocomposites with different ITO concentrations at low and high magnifications: (a, b) 35 wt %; (c, d) 20 wt %; (e, f) 10 wt %.

azide groups have reacted.⁵² The increasing carbon content in the quantitative XPS analysis also indicated the successful grafting of PGMA chains.

Figure 6 presents the TGA curve for the synthesized particles, phosphate treated particles, and PGMA grafted particles. Approximately 10% weight loss in the as-synthesized particles was due to the loss of the surface capping oleic acid. The increase in weight loss for the phosphate–azide treated ITO particles and ITO/PGMA particles presents further evidence for successful surface treatment of the phosphate ligand and grafting of the PGMA chains. It is noteworthy that compared with the ITO particles treated with small ligands, the PGMA grafted particles showed stronger steric stability against agglomeration. Figure 7 is

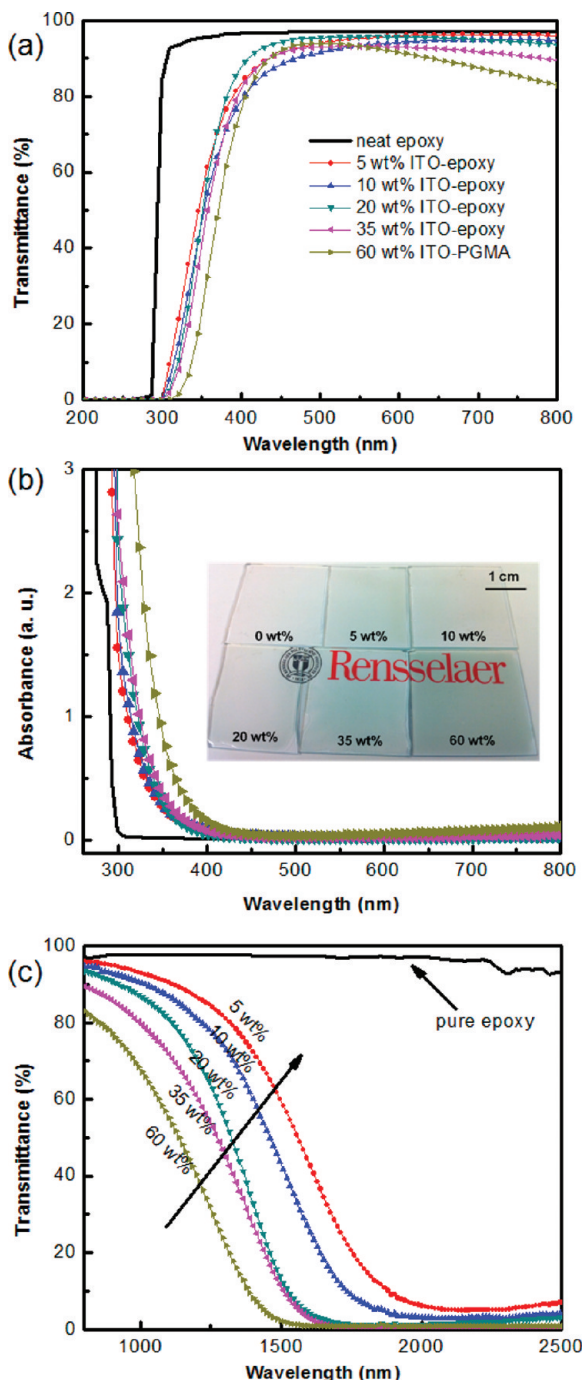


Figure 9. UV-vis spectra of ITO/epoxy nanocomposites with different ITO contents (a) transmittance and (b) absorbance (the inset pictures are digital photographs of $20\text{ }\mu\text{m}$ thick ITO/epoxy coating on glass substrate with thickness); (c) near IR transmittance spectra of ITO/epoxy nanocomposites.

a digital photograph of the stable dispersion of PGMA grafted ITO nanoparticles within chloroform solvent, coating on a glass substrate and self-standing composites after removal of solvent. It can be seen that the grafted particles formed a transparent dispersion, highly transparent coatings, and transparent self-supporting film. With 60 wt % loading of particles, the grafted PGMA polymer chains effectively screened the ITO nanoparticle core–core attraction and transparent composites were obtained.

However, physical blending ITO particles with PGMA polymers suffered from severe agglomeration and transparent composites were not obtained. The grafted ITO nanoparticles could be mixed with epoxy resin without agglomeration. Figure 7d shows the highly transparent green color 20 wt % loaded ITO/epoxy composite sample with a thickness of 3 mm after removing the solvent and curing.

Figure 8 shows the TEM images of ITO/epoxy nanocomposites with PGMA grafted ITO nanoparticles at different loading levels. Both the low and high magnification micrographs show that the ITO nanoparticles are homogeneously dispersed in the epoxy matrix and agglomerates were absent. Within the higher loading samples, the particles are more densely distributed. The chemical similarity of the grafted polymer chains with the matrix polymer minimized the mixing enthalpy. Additionally, the long grafted PGMA polymer chains can be swollen and wetted by the small matrix epoxy molecules, and this is beneficial for good dispersion of ITO particles within epoxy matrix.^{37,53}

Figure 9a,b shows the transmittance and absorbance spectra of ITO nanocomposites at several loadings with a thickness about $20\text{ }\mu\text{m}$ coated on glass substrates. In the visible range (400–800 nm), the ITO composites show more than 90% transparency. Similar to the transmittance spectrum of as-synthesized ITO dispersion in solvent, ITO/epoxy composites with high ITO concentration show slightly decreased transmittance of visible light from 500 to 800 nm. This is also consistent with increased absorption in the absorbance spectra. In the UV range, the neat epoxy only blocks UV light up to 300 nm. The ITO/epoxy nanocomposites block UV light in the 300–400 nm range, and high loading samples show stronger absorption of UV light. TiO₂ and ZnO nanoparticles are well-known to be useful in UV protection for organic polymers even with very low loading fraction. Unlike TiO₂ and ZnO intrinsic semiconductor nanoparticles, ITO particles, as a degenerate semiconductor, do not have a very sharp UV absorption edge. The resultant ITO/epoxy composites show a relatively broad absorption in the 300–400 nm range. As shown in the transmittance spectra, ITO nanoparticles at 5 wt % content in the epoxy resin showed a 60% shielding efficiency of UV light at $\sim 350\text{ nm}$ and more than 90% transparency of the whole visible light. The introduction of matrix compatible polymer chain grafted ITO nanoparticles increased the UV shielding ability of epoxy resin from 300 to 400 nm but maintained high optical transparency feature of epoxy in the visible light range.

As shown in the inset photographs, the composite coatings are highly transparent and no visible clouding was observed for all the samples. The only difference is that the samples with high ITO content appear more greenish. The high optical clarity of the prepared composites can be attributed to the good dispersion of the grafted ITO nanoparticles within the epoxy matrix, which minimizes the scattering loss. The loss of transparency of nanoparticle filled polymer composites due to scattering can be estimated from the equation below^{6,12,14}

$$T = \frac{I}{I_0} = \exp \left(- \left[\frac{3\varphi_p x r^3}{4\lambda^4} \left(\frac{n_p}{n_m} - 1 \right) \right] \right) \quad (2)$$

where I and I_0 are the transmitted and incident light intensity, r is the radius of spherical particles, φ_p is the volume fraction of inorganic particles, x is the optical path length, λ is the wavelength of incident light, and n_p and n_m are the refractive index of particles (ITO, $n \approx 1.9$) and polymer matrix (epoxy, $n \approx 1.5$),

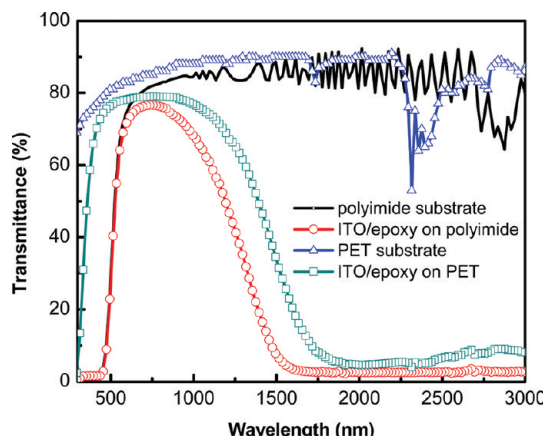


Figure 10. UV–vis–NIR transmittance spectra of 35 wt % ITO-epoxy coating (with thickness of 5 μm) on plastic substrates.

respectively. Equation 2 shows that controlling the dispersion of the inorganic nanoparticles within polymer matrix is critical to achieve high optical transparency of prepared composites. When the ITO/epoxy nanocomposites prepared here are referred to, the matrix compatible polymer chains grafted on ITO nanoparticles prevent the formation of large agglomerates. The true ITO nanoparticles (6.3 nm in diameter based on TEM observations) are significantly smaller than visible light wavelengths and, therefore, optical scattering was suppressed. As a result, as shown in Figure 9a, the ITO/epoxy thin film coatings were highly transparent and the transparency did not deteriorate with increasing ITO content from 5 wt % to 35 wt %.

Figure 9c presents the near-infrared transmittance spectra of ITO/epoxy nanocomposites as a function of wavelength in comparison with neat epoxy on a glass substrate in the 800–2500 nm wavelength range. The neat epoxy resin showed a constant more than 97% transmittance in the whole IR range. Only several weak functional group absorption peaks associated with epoxy polymer were observed in the long IR range. In contrast, all the ITO/epoxy composite films show low transmittance in the IR range. The IR transmission cutoff wavelength of the ITO/epoxy coatings shifts toward shorter wavelength with increasing content of ITO nanoparticles. Tin-doped In_2O_3 is a heavily doped n-type semiconductor and known to be opaque in the near-infrared, because of the free carrier absorption within the conduction band.^{54,55} The IR-shielding efficiency was primarily determined by the free carrier concentration within the sample. It can be understood that, based on the Beer–Lambert law, the interaction of the IR light with the sample increases with free electron concentration. The 60 wt % ITO sample shows near 100% IR shielding efficiency, and progressively lowering the ITO concentration decreases the IR shielding ability. Therefore, in order to screen the IR effectively, a relatively high concentration of ITO nanoparticles is desired. Luo et al. reported a 10% enhancement of IR shielding efficiency of 0.08 wt % Al-doped ZnO /epoxy with 3 mm thickness over neat epoxy matrix.¹⁴ In contrast, the 5 wt % ITO/epoxy thin film composites with a thickness around 20 μm effectively blocked more than 90% of the IR light at wavelength longer than 2000 nm.

Furthermore, the ITO/epoxy nanocomposite coatings were applied on polyimide and polyethylene terephthalate (PET) plastic substrate at ambient conditions with the common spin-coating method. The film on a flexible substrate also exhibited

high transparency in the visible range, strong UV absorption, and high IR shielding ability. Figure 10 shows the UV–vis–NIR transmission spectra of 5 μm thick ITO/epoxy (35 wt %) coating on polyimide and PET substrates in comparison to the uncoated substrates. The thin film interference effect of the polyimide can be seen in the uncoated thin film substrate. After applying ITO/epoxy coating, in the near IR range, the sample shows zero transmittance. Due to the strong absorption of light around 500 nm, the ITO-epoxy coated polyimide showed a similar absorption edge as the polyimide substrate. The UV absorption property of ITO-epoxy composites in the 300–400 nm range was shown on the coating of PET substrate. Meanwhile, the intrinsic vibration and stretching of the functional group in PET in the IR range was totally masked with ITO/epoxy coating. The high optical transparency in the visible light range for both polyimide and PET substrates were retained with the homogeneously dispersed ITO/epoxy coating.

4. CONCLUSIONS

In this work, homogeneous dispersion of ITO nanoparticles within a commercial epoxy matrix was achieved by grafting epoxy compatible poly (glycidyl methacrylate) (PGMA) chains onto the surface of ITO particles via a combination of phosphate ligand engineering and Cu(I) catalyzed alkyne–azide “click” chemistry. The prepared ITO/epoxy nanocomposites show more than 90% transparency of visible light and absorb UV light in the range of 300–400 nm. The ITO/epoxy composites demonstrate low transmittance of near-infrared light, and increasing the ITO concentration leads to higher IR shielding efficiency. The ITO/epoxy composites can be easily applied onto glass and flexible plastic substrates to behave as functional optical coatings. To summarize, tailoring the interface of ITO nanoparticles by grafting matrix compatible polymer chains is a facile and effective way to prepare visibly transparent, UV/IR opaque ITO polymer nanocomposites.

■ AUTHOR INFORMATION

Corresponding Author

*E-mail: Schadl@rpi.edu.

■ ACKNOWLEDGMENT

This work was supported by the Engineering Research Center Program (ERC) of the National Science Foundation under Cooperative Agreement EEC-0812056 and in part by New York State under NYSTAR contract C090145. The authors also acknowledge financial support by the Nanoscale Science and Engineering Initiative of the National Science Foundation under NSF award number DMR-0642573.

■ REFERENCES

- (1) Gazotti, W. A.; Casalbore-Miceli, G.; Geri, A.; Berlin, A.; Paoli, M. A. D. *Adv. Mater.* **1998**, *10*, 1522–1525.
- (2) Pichot, F.; Ferrere, S.; Pitts, R. J.; Gregg, B. A. *J. Electrochem. Soc.* **1999**, *146*, 4324–4326.
- (3) Lewis, B. G.; Paine, D. C. *MRS Bull.* **2000**, *25*, 22–27.
- (4) Gordon, R. G. *MRS Bull.* **2000**, *52*–57.
- (5) Betz, U.; Kharrazi Olsson, M.; Marthy, J.; Escolá, M. F.; Atamny, F. *Surf. Coat. Technol.* **2006**, *200*, 5751–5759.
- (6) Caseri, W. *Chem. Eng. Commun.* **2009**, *196*, 549–572.

- (7) Althues, H.; Henle, J.; Kaskel, S. *Chem. Soc. Rev.* **2007**, *36*, 1454–65.
- (8) Ajayan, P. M.; Schadler, L. S.; Braun, P. B. *Nanocomposite Science and Technology*; Wiley VCH: Weinheim, Germany, 2003.
- (9) May, C. A., Ed. *Epoxy Resin: Chemistry and Technology*; Dekker: New York, 1976, p 485.
- (10) Sun, D.; Sue, H.-J.; Miyatake, N. *J. Phys. Chem. C* **2008**, *112*, 16002–16010.
- (11) Yang, Y.; Li, Y.-Q.; Fu, S.-Y.; Xiao, H.-M. *J. Phys. Chem. C* **2008**, *112*, 10553–10558.
- (12) Koziej, D.; Fischer, F.; Kränzlin, N.; Caseri, W. R.; Niederberger, M. *ACS Appl. Mater. Interfaces* **2009**, *1*, 1097–1104.
- (13) Tu, Y.; Zhou, L.; Jin, Y. Z.; Gao, C.; Ye, Z. Z.; Yang, Y. F.; Wang, Q. *L. J. Mater. Chem.* **2010**, *20*, 1594.
- (14) Luo, Y.-S.; Yang, J.-P.; Dai, X.-J.; Yang, Y.; Fu, S.-Y. *J. Phys. Chem. C* **2009**, *113*, 9406–9411.
- (15) Granqvist, C. G.; Hultåker, A. *Thin Solid Films* **2001**, *411*, 1–5.
- (16) Zheng, J. P.; Kwok, H. S. *Appl. Phys. Lett.* **1993**, *63*, 1–3.
- (17) Ni, J.; Yan, H.; Wang, A.; Yang, Y.; Stern, C. L.; Metz, A. W.; Jin, S.; Wang, L.; Marks, T. J.; Ireland, J. R.; Kannewurf, C. R. *J. Am. Chem. Soc.* **2005**, *127*, 5613–5624.
- (18) Kim, J. K.; Chhajed, S.; Schubert, M. F.; Schubert, E. F.; Fischer, A. J.; Crawford, M. H.; Cho, J.; Kim, H.; Sone, C. *Adv. Mater.* **2008**, *20*, 801–804.
- (19) Canhola, P.; Martins, N.; Raniero, L.; Pereira, S.; Fortunato, E.; Ferreira, I.; Martins, R. *Thin Solid Films* **2005**, *487*, 271–276.
- (20) Goebbert, C.; Nonninger, R.; Aegeerter, M. A.; Schmidt, H. *Thin Solid Films* **1999**, *351*, 79–84.
- (21) Al-Dahoudi, N.; Aegeerter, M. A. *J. Sol-Gel. Sci. Technol.* **2003**, *26*, 693–697.
- (22) Ederth, J.; Heszler, P.; Hultåker, A.; Niklasson, G. A.; Granqvist, C. G. *Thin Solid Films* **2003**, *445*, 199–206.
- (23) Yin, Y.; Zhou, S.; Gu, G.; Wu, L. *J. Mater. Sci.* **2007**, *42*, 5959–5963.
- (24) Chatterjee, S. *J. Mater. Sci.* **2008**, *43*, 1696–1700.
- (25) Miyazaki, H.; Ota, T.; Yasui, I. *Sol. Energy Mater. Sol. Cells* **2003**, *79*, 51–55.
- (26) Ba, J.; Fattakhova Rohlfsing, D.; Feldhoff, A.; Brezesinski, T.; Djerdj, I.; Wark, M.; Niederberger, M. *Chem. Mater.* **2006**, *18*, 2848–2854.
- (27) Bühl, G.; Thölmann, D.; Feldmann, C. *Adv. Mater.* **2007**, *19*, 2224–2227.
- (28) Sun, Z.; He, J.; Kumbhar, A.; Fang, J. *Langmuir* **2010**, *26*, 4246–4250.
- (29) Choi, S.-I.; Nam, K. M.; Park, B. K.; Seo, W. S.; Park, J. T. *Chem. Mater.* **2008**, *20*, 2609–2611.
- (30) Capozzi, C. J.; Gerhardt, R. A. *Adv. Funct. Mater.* **2007**, *17*, 2515–2521.
- (31) Neouze, M.-A.; Schubert, U. *Monatsh. Chem.* **2008**, *139*, 183–195.
- (32) Hu, Y.; Gu, G.; Zhou, S.; Wu, L. *Polymer* **2011**, *52*, 122–129.
- (33) Frickel, N.; Messing, R.; Gelbrich, T.; Schmidt, A. M. *Langmuir* **2010**, *26*, 2839–2846.
- (34) Mutin, P. H.; Guerrero, G.; Vioux, A. *J. Mater. Chem.* **2005**, *15*, 3761–3768.
- (35) Kang, M.-S.; Ma, H.; Yip, H.-L.; Jen, A. K.-Y. *J. Mater. Chem.* **2007**, *17*, 3489.
- (36) Xu, C.; Ohno, K.; Ladmiral, V.; Composto, R. J. *Polymer* **2008**, *49*, 3568–3577.
- (37) Akcora, P.; Liu, H.; Kumar, S. K.; Moll, J.; Li, Y.; Benicewicz, B. C.; Schadler, L. S.; Acehan, D.; Panagiotopoulos, A. Z.; Pryamitsyn, V.; Ganesan, V.; Ilavsky, J.; Thiagarajan, P.; Colby, R. H.; Douglas, J. F. *Nat. Mater.* **2009**, *8*, 354–359.
- (38) Ranjan, R.; Brittain, W. J. *Macromol. Rapid Commun.* **2007**, *28*, 2084–2089.
- (39) Barbey, R.; Lavanant, L.; Paripovic, D.; Schüwer, N.; Sugnaux, C.; Tugulu, S.; Klok, H.-A. *Chem. Rev.* **2009**, *109*, 5437–5527.
- (40) Kim, J. U.; Matsen, M. W. *Macromolecules* **2008**, *41*, 246–252.
- (41) White, M. A.; Johnson, J. A.; Koberstein, J. T.; Turro, N. J. *J. Am. Chem. Soc.* **2006**, *128*, 11356–11357.
- (42) Lu, X.; Sun, F.; Wang, J.; Zhong, J.; Dong, Q. *Macromol. Rapid Commun.* **2009**, *30*, 2116–2120.
- (43) Dach, B. I.; Rengifo, H. R.; Turro, N. J.; Koberstein, J. T. *Macromolecules* **2010**, *43*, 6549–6552.
- (44) Achatz, D. E.; Heilitag, F. J.; Li, X.; Link, M.; Wolfbeis, O. S. *Sens. Actuators, B: Chem.* **2010**, *150*, 211–219.
- (45) Ranjan, R.; Brittain, W. J. *Macromolecules* **2007**, *40*, 6217–6223.
- (46) Li, C.; Han, J.; Ryu, C. Y.; Benicewicz, B. C. *Macromolecules* **2006**, *39*, 3175–3183.
- (47) Gilstrap, R. A.; Capozzi, C. J.; Carson, C. G.; Gerhardt, R. A.; Summers, C. *J. Adv. Mater.* **2008**, *20*, 4163–4166.
- (48) Li, Y.; Benicewicz, B. C. *Macromolecules* **2008**, *41*, 7986–7992.
- (49) Kim, P.; Jones, S. C.; Hotchkiss, P. J.; Haddock, J. N.; Kippelen, B.; Marder, S. R.; Perry, J. W. *Adv. Mater.* **2007**, *19*, 1001–1005.
- (50) Collman, J. P.; Devaraj, N. K.; Eberspacher, T. P. A.; Chidsey, C. E. D. *Langmuir* **2006**, *22*, 2457–2464.
- (51) Daugaard, A. E.; Hvilsted, S.; Hansen, T. S.; Larsen, N. B. *Macromolecules* **2008**, *41*, 4321–4327.
- (52) Goldmann, A. S.; Walther, A.; Nebhani, L.; Joso, R.; Ernst, D.; Loos, K.; Barner-Kowollik, C.; Barner, L.; Muller, A. H. E. *Macromolecules* **2009**, *42*, 3707–3714.
- (53) Smith, G. D.; Bedrov, D. *Langmuir* **2009**, *25*, 11239–11243.
- (54) Ederth, J.; Johnsson, P.; Niklasson, G.; Hoel, A.; Hultåker, A.; Heszler, P.; Granqvist, C.; Doorn, A. R.; Jongerius, M.; Burgard, D. *Phys. Rev B* **2003**, *68*, 1–10.
- (55) Kanehara, M.; Koike, H.; Yoshinaga, T.; Teranishi, T. *J. Am. Chem. Soc.* **2009**, *131*, 17736–17737.